UNIVERSITY
OF TRENTO

DIPARTIMENTO DI INGEGNERIA E SCIENZA DELL'INFORMAZIONE

38123 Povo – Trento (Italy), Via Sommarive 14
http://www.disi.unitn.it

A FINITE ELEMENT PROCEDURE BASED ON A BOUNDARY
VALUE APPROACH FOR THE EVALUATION OF THE
ELECTROMAGNETIC EXPOSURE IN BIOLOGICAL PHANTOMS

S. Caorsi, E. Bermani, and A. Massa

January 2011

Technical Report # DISI-11-093

A Finite Element Procedure Based on a Boundary Value Approach for the Evaluation of the Electromagnetic Exposure in Biological Phantoms

S. Caorsi[*], E. Bermani[*] and A. Massa[**]

[*] Dept. of Electronics, University of Pavia, Via Ferrata 1, I-27100, Pavia, Italy

[**] Dept. of Information and Communication Technology, University of Trento, Via Mesiano 77, I-38050, Trento, Italy

Abstract - In this paper, a finite element method, based on a boundary value approach, for the evaluation of the electric field distribution in exposed biological phantoms is presented. Starting from the measurement of the electric field around the phantom, the field prediction is obtained by solving a boundary value problem. This allows to avoid the description of the electromagnetic source and the estimation of the electric field distribution also when the illuminating source is unknown or when its numerical model is not available. In order to show the effectiveness of the proposed approach, some numerical results, concerning a two dimensional geometry, are provided. Firstly, the accuracy and validity of the electromagnetic prediction are assessed by comparing numerical with reference solutions (analytically computed). Then, in order to demonstrate the efficiency, the robustness and capability of this technique, different measurement strategies, noisy environments and errors in the data acquisition are taken into account.

I. INTRODUCTION

In response to continued and growing public concerns on possible adverse health effects of electric, magnetic and electromagnetic fields, many research activities have been carried out over the last years. Earlier studies were mainly focused upon ELF [1]-[3] in public environments, such as high voltages lines and household appliances, and in occupational environments. However, because of the rapid development and deployment of mobile and wireless communications, the focus has been recently largely shifted towards higher frequencies. Several direct approaches have been developed to evaluate the electromagnetic exposure to RF and to microwave frequencies. Analytic solutions [4]-[6] as well as numerical techniques, such as the method of moment [7], the finite element method [8]-[9], some hybrid methods [10]-[12] and, in particular, the finite difference method [13]-[17], have been taken into account. These approaches allow to obtain a good accuracy in the estimation of the electromagnetic field distribution in a given phantom when an accurate model of the radiating source is available.

However, in some situations, a numerical description of the illuminating source could be difficult and, in other cases (for instance, if the e.m. source is completely unknown) even impossible. In these situations, the evaluation of the electromagnetic field could be a challenging problem. It has been shown [18]-[22] that different e.m. sources (i.e. electromagnetic sources differing in shape, position, radiation pattern, …) as well as the choice of a specific numerical model of the

illumination source produce not negligible variations in the e.m. field distribution induced in a fixed biological structure.

For this reason and for those conditions, numerical approaches, avoiding the numerical modeling of the illumination source, results certainly very attractive.

Recently, *Caorsi and Massa* [23]-[24] faced the problem by considering an *inverse* approach based on a microwave imaging technique. The method allows to predict the electric field distribution in a given biological structure through the minimization of a suitably defined cost function. The numerical modeling of the e.m. source is avoided by employing the complex [24] or the amplitude-only [25] values of the scattered electric field, measured around the phantom, and those of the incident field, collected in the investigation domain.

In this paper, an alternative solution, based on a *direct* approach, is presented. The proposed approach evaluates the induced electromagnetic field starting from the knowledge of the tangential component of the electric field around the biological phantom and solving a direct electromagnetic problem. By choosing a proper numerical domain and by considering the measurement data as boundary conditions, the problem is formulated in terms of a boundary value problem. No description of the illuminating source is required. The e.m. source is completely described by means of the values of the tangential component of the total electric field measured on the boundary.

In the following, the proposed technique is illustrated and deeply assessed. The dependence of the accuracy in the field prediction on the number of measurement points and the robustness of the approach to noisy input data are checked by means of selected numerical examples. Furthermore, the presence of possible errors in the positioning of the data acquisition system is taken into account.

II. MATHEMATICAL FORMULATION

Let us consider the geometry shown in Figure 1. An electromagnetic source illuminates a biological structure characterized by a known dielectric permittivity $\varepsilon_{b.s.}(\mathbf{r})$ and an electric conductivity $\sigma_{b.s.}(\mathbf{r})$. The object is located inside a host medium whose dielectric parameters are $\varepsilon_{h.m.}(\mathbf{r})$ and $\sigma_{h.m.}(\mathbf{r})$. The magnetic permeability is everywhere that of the free-space.
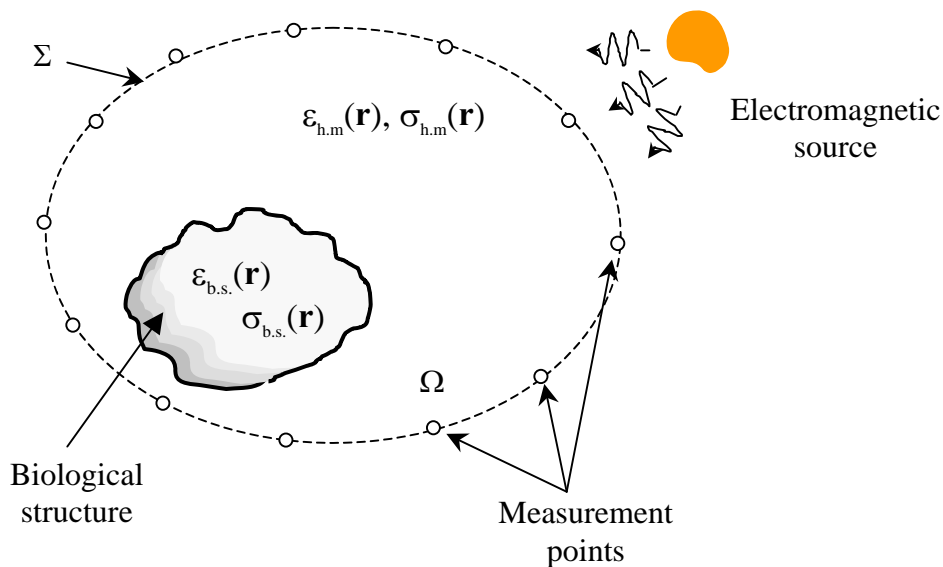
Fig. 1 Problem geometry.

Let Σ be a closed surface defining a region Ω (investigation region) to which the biological structure belongs. Moreover let the illumination source be external to the investigation region.

Starting from the knowledge of tangential component of the electric field on Σ, the evaluation of the electric field distribution inside the biological structure can be formulated as a boundary value problem

$$\begin{cases} \nabla \times \nabla \times \mathbf{E}(\mathbf{r}) - \omega^2 \varepsilon(\mathbf{r}) \mu_o \mathbf{E}(\mathbf{r}) = 0 & \text{in } \Omega \\ \mathbf{n} \times \mathbf{E}(\mathbf{r}) = \mathbf{g}(\mathbf{r}) & \text{on } \Sigma \end{cases} \tag{1}$$

where $\mathbf{n}$ indicates the outward normal vector on Σ, $\varepsilon(\mathbf{r})$ is the complex dielectric permittivity and $\mathbf{g}(\mathbf{r})$ is a given vectorial function defined on Σ.

The problem in (1) is well posed. Moreover, the illuminating source is completely described by means of boundary conditions (i.e., the value of the tangential component of $\mathbf{E}(\mathbf{r})$ on Σ). This allows to obtain the distribution of the electric field inside the whole biological structure as the unique solution of (1) without requiring any modeling of the electromagnetic source [26].

In order to numerically solve (1), a finite element approach is considered. By assuming two different weighting functions $\mathbf{w}$ and $\overline{\mathbf{w}}$, a variational formulation of (1) is firstly obtained

$$\int_\Omega \left[\nabla \times \mathbf{E}(\mathbf{r}) \cdot \nabla \times \mathbf{w}(\mathbf{r}) - \omega^2 \varepsilon(\mathbf{r}) \mu_o \mathbf{E}(\mathbf{r}) \cdot \mathbf{w}(\mathbf{r}) \right] d\Omega =$$
$$= \int_\Sigma [\mathbf{n} \times \nabla \times \mathbf{E}(\mathbf{r})] \cdot \mathbf{w}(\mathbf{r}) d\Sigma + \int_\Sigma [\mathbf{n} \times \mathbf{E}(\mathbf{r}) - \mathbf{g}(\mathbf{r})] \cdot \overline{\mathbf{w}}(\mathbf{r}) d\Sigma \tag{2}$$

By choosing the weighting function $\mathbf{w}(\mathbf{r})$ so that it vanishes on Σ and by imposing that the electric field distribution $\mathbf{E}(\mathbf{r})$ satisfies the weighted boundary condition on Σ for each $\overline{\mathbf{w}}(\mathbf{r})$, eq. (2) can be re-written as

$$\int_\Omega \left[\nabla \times \mathbf{E}(\mathbf{r}) \cdot \nabla \times \mathbf{w}(\mathbf{r}) - \omega^2 \varepsilon(\mathbf{r}) \mu_o \mathbf{E}(\mathbf{r}) \cdot \mathbf{w}(\mathbf{r}) \right] d\Omega = 0 \tag{3}$$

Then, a finite element space discretization of (3) is obtained by introducing a triangulation $\boldsymbol{\tau}_h$ of $\overline{\Omega}$ (where $\overline{\Omega} = \Omega \cup \Sigma$) and by defining a specific finite element basis $V = \{\mathbf{v}_i(\mathbf{r}), i = 1,..., m\}$ on $\boldsymbol{\tau}_h$, which spans a finite dimensional subspace $V_h \in \mathrm{H}(\mathrm{curl};\Omega)$ (where

$$\mathrm{H}(\mathrm{curl};\Omega) = \left\{ \mathbf{w}(\mathbf{r}): \int_\Omega |\mathbf{w}(\mathbf{r})|^2 d\Omega < +\infty \text{ and } \int_\Omega |\nabla \times \mathbf{w}(\mathbf{r})|^2 d\Omega < +\infty \right\}$$ being h the maximum diameter

of the elements of the triangulation $\boldsymbol{\tau}_h$).

Let us express $\mathbf{E}(\mathbf{r})$ as a linear combination of the finite element basis

$$\mathbf{E}(\mathbf{r}) = \sum_{i=1}^m e_i \, \mathbf{v}_i(\mathbf{r}) \tag{4}$$

By imposing that (3) holds for each $\mathbf{w}_j(\mathbf{r}) \in W$, where $W = \{\mathbf{w}_j(\mathbf{r}), j = 1,..., k: \mathbf{w}_j(\mathbf{r}) \in V_h, \mathbf{w}_j(\mathbf{r}) = 0 \text{ on } \Sigma\}$, the following system is obtained:

$$\sum_{i=1}^{m} \int_{\Omega} e_i \Big[\nabla \times \mathbf{v}_i(\mathbf{r}) \cdot \nabla \times \mathbf{w}_j(\mathbf{r}) - \omega^2 \varepsilon(\mathbf{r}) \mu_o e_i \, \mathbf{v}_i(\mathbf{r}) \cdot \mathbf{w}_j(\mathbf{r}) \Big] \, d\Omega = 0 \qquad \forall \mathbf{w}_j(\mathbf{r}) \in W$$

(5)

In a matrix form, it can be rewritten as

$$\Big[\mathbf{S}_{jf} - \omega^2 \mu_o \mathbf{T}_{jf} \Big] \mathbf{e}_f = - \Big[\mathbf{S}_{jp} - \omega^2 \mu_o \mathbf{T}_{jp} \Big] \mathbf{e}_p$$

(6)

where $\mathbf{e}_f$ and $\mathbf{e}_p$ are the array of the unknown coefficients and the array of known boundary coefficients, respectively; the matrix elements $S_{j,i}$ and $T_{j,i}$ are defined as

$$S_{j,i} = \int_{\Omega} \nabla \times \mathbf{v}_i(\mathbf{r}) \cdot \nabla \times \mathbf{w}_j(\mathbf{r}) \, d\Omega$$

(7)

$$T_{j,i} = \int_{\Omega} \varepsilon(\mathbf{r}) \, \mathbf{v}_i(\mathbf{r}) \cdot \mathbf{w}_j(\mathbf{r}) \, d\Omega$$

(8)

where 9 verify $\mathbf{v}_f(\mathbf{r}) = 0$ and $\mathbf{v}_p(\mathbf{r}) \neq 0$ on Σ, respectively.

Because of the linear algebraic system (6) is well conditioned [27], the solution can be obtained by means of a standard numerical technique [28]. As far as basis and test functions are concerned ($\mathbf{v}_i; i = 1,...,m$ and $\mathbf{w}_j; j = 1,...,k$, respectively), edge elements [29] are generally used when vectorial problems are addressed. Nonetheless, linear Lagrange basis functions [27] can be considered when scalar formulation are handled.

III. NUMERICAL RESULTS

In order to preliminary assess the effectiveness of the proposed approach, a test case, for which an analytical reference solution is available, is analyzed.
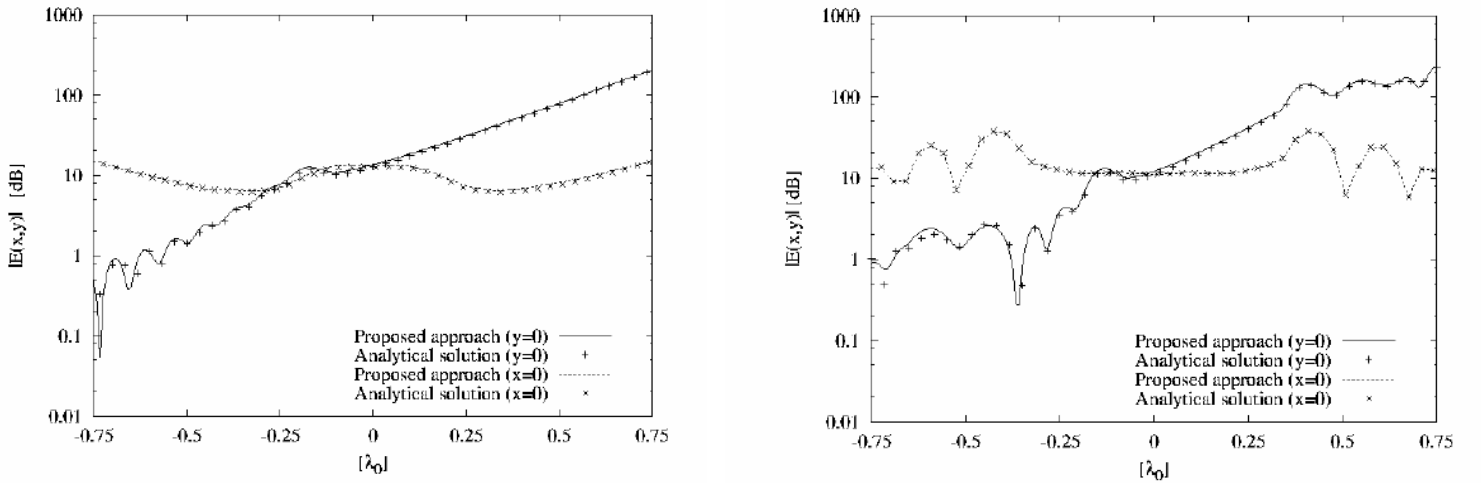
(a)   (b)

Fig. 2 Amplitude of the electric field along the x-axis and the y-axis. (*a*) Homogeneous cylinder; (*b*) Multi-layer cylinder.

A circular cylinder, illuminated by an infinite electric line positioned $1.5\lambda_o$ far from the object (being λ_o the wavelength in free-space), is considered. The axis of the cylinder is coincident with the z-axis and its radius is equal to $0.75\lambda_o$. The investigation domain is a square region $l=2.4\lambda_o$ in side, non-coaxial with the dielectric cylinder, and Σ is its boundary. In order to discretize $\overline{\Omega}$, a triangular mesh is obtained starting from an uniform grid with square elements $\Delta_b = 0.0125\lambda_o$-sided. Basis functions are lagrangian elements [27]. The values of the tangential component of $\mathbf{E}(\mathbf{r})$ are analitically computed at M measurement points coincident with all the boundary nodes on Σ.

Figures 2(*a*) and 2(*b*) show the amplitude of the electric field, along both the x-axis and the y-axis, for a homogeneous ($\varepsilon_r = 40.0$ and $\sigma = 0.5$ S/m) and for a stratified dielectric cylinder (inner layer: $\varepsilon_{r1} = 55.0$, $\sigma_1 = 0.9$ S/m; medium layer: $\varepsilon_{r2} = 12.0$, $\sigma_2 = 0.1$ S/m; external layer $\varepsilon_{r3} = 41.0$, $\sigma_3 = 0.8$ S/m), respectively. For comparison, also analytical solutions are reported.

In order to quantitatively evaluate the prediction accuracy, some error figures are defined as follows:

$$\xi(x_n, y_n) = \frac{\left\| \mathbf{E}_{act}(x_n, y_n) \right| - \left| \mathbf{E}_{pred}(x_n, y_n) \right\|}{\left| \mathbf{E}_{act}(x_n, y_n) \right|} \qquad \forall n = 1...N \qquad (Amplitude\ Error) \qquad (9)$$

$$\phi(x_n, y_n) = \frac{\left| ph_{act}\{\mathbf{E}(x_n, y_n)\} - ph_{pred}\{\mathbf{E}(x_n, y_n)\} \right|}{2\pi} \qquad \forall n = 1...N \qquad (Phase\ Error) \qquad (10)$$

where (x_n, y_n) indicates the position of the n-*th* node of the mesh belonging to the biological body; N is the number of nodes inside the biological body; the subscripts *act* and *pred* indicate actual and predicted values, respectively; $\left| \mathbf{E}(x, y) \right|$ and $ph\{\mathbf{E}(x, y)\}$ are the amplitude and the phase of the electric field, respectively.
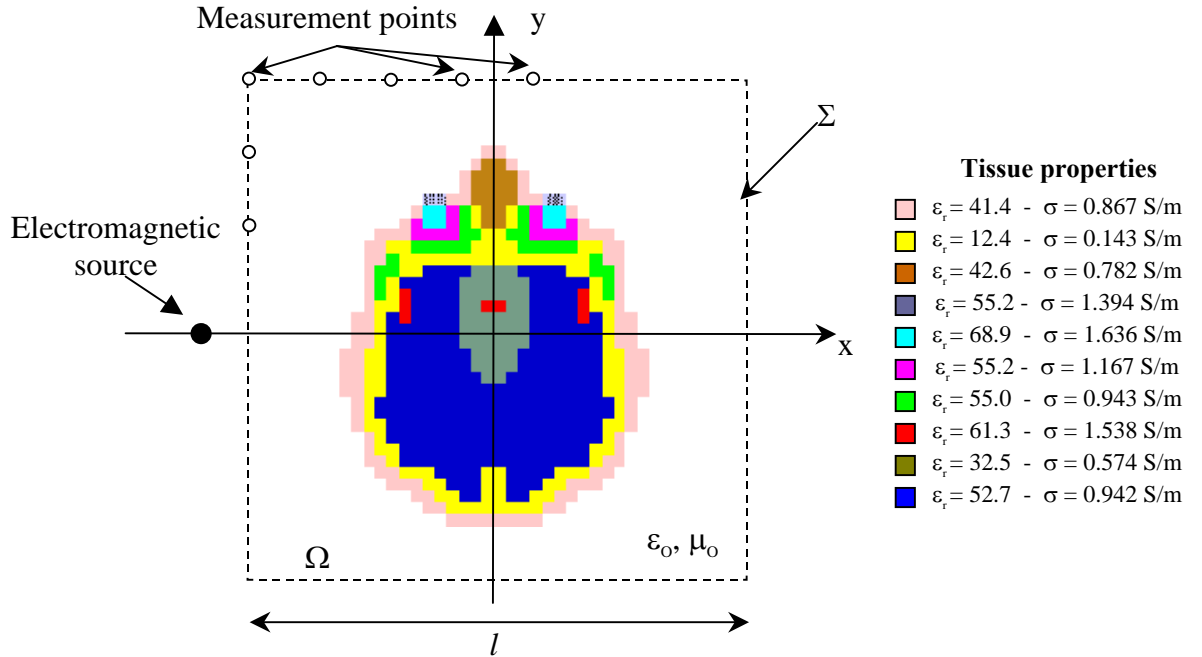
Fig. 3   Model of the biological phantom.

As far as the first example is concerned, the average amplitude error $av\{\xi(x, y)\}$ is equal to –87.1dB, for the homogeneous cylinder, and to -85.7dB, for the stratified one. The average phase errors $av\{\phi(x, y)\}$ are $2.18 \cdot 10^{-5}$ and $1.66 \cdot 10^{-5}$, respectively.

The second test case is devoted to analyze a more complex structure. A discretized version of a horizontal slice of a human head, located in the vacuum, is assumed as biological phantom (Figure 3). In this example, Ω is a square region $l=0.648\lambda_o$ discretized with triangular elements starting from an uniform grid of square elements $\Delta_b=0.018\lambda_o$ in size. The values of the tangential component of $\mathbf{E}(\mathbf{r})$ are collected at M measurement points uniformly distributed along Σ.


(a)

(b)

(c)

(d)
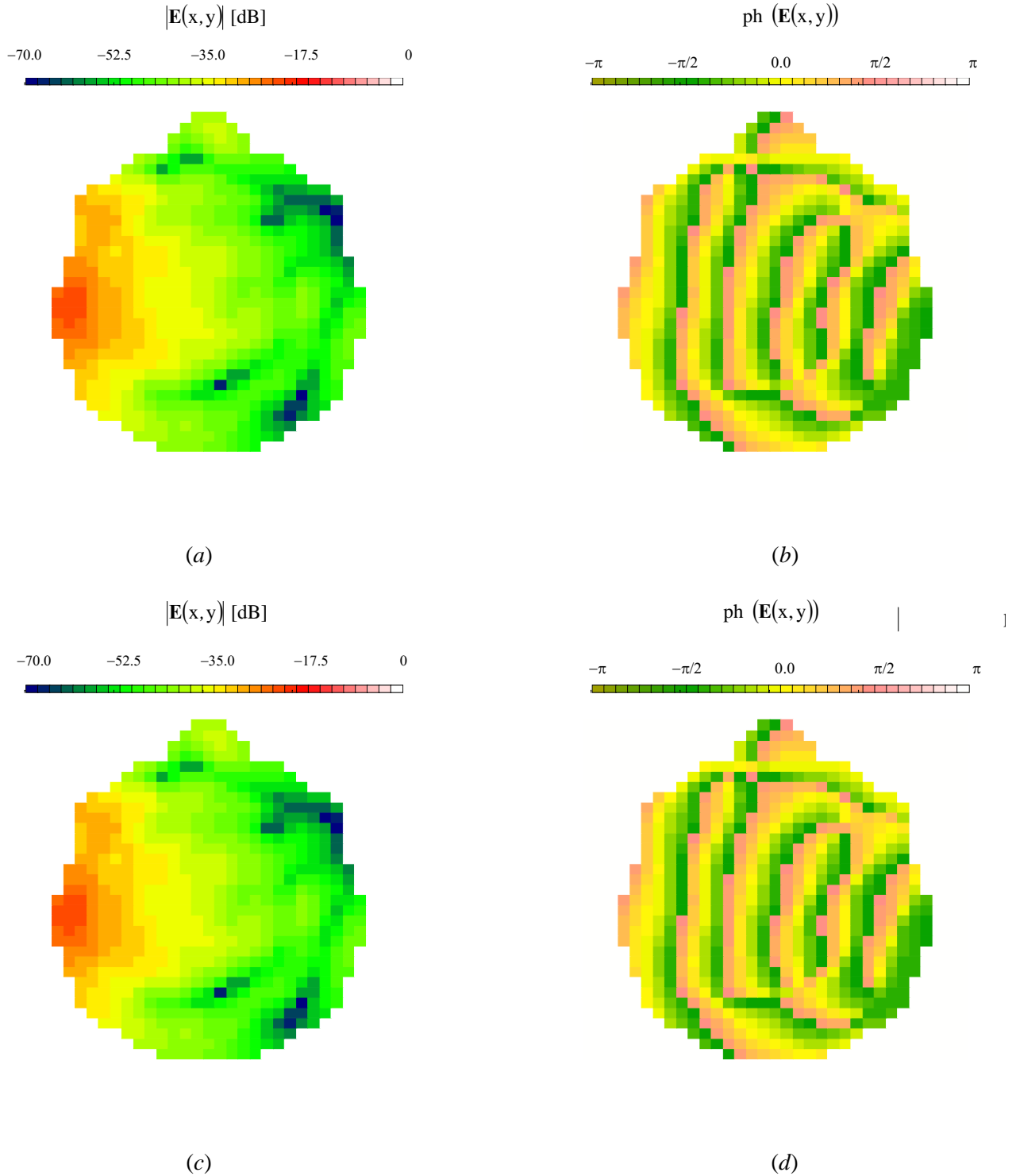
Fig. 4 Electric field distribution. Estimated field distribution (M = 144): amplitude (a) and phase (b). Reference distribution: amplitude (c) and phase (d).

Input data are synthetically generated by considering a larger discretization domain ($l_u=1.98\lambda_o$), with different mesh size ($\Delta_u = \Delta_b/2$), illuminated by an infinite electric line, located $0.126\lambda_o$ far from the biological structure. The computational domain is limited by means of an anisotropic perfectly matched layer [30].

Firstly, the electric field distribution inside the biological structure is computed by considering the measurement points coincident with all the boundary nodes. Figures 4(*a*) and 4(*b*) show the amplitude and phase of the predicted field, respectively. By comparing estimated distributions with the actual values (shown in Figure 4(*c*) and 4(*d*)), a good agreement can be observed in the whole biological structure. The average amplitude error $av\{\xi(x,y)\}$ is equal to -89.9dB and the average phase error $av\{\phi(x,y)\}$ is $2.28\cdot10^{-5}$. These indications clearly confirm that, if the number of measurement points is equal to that of the boundary nodes and if the measurement points are located at the boundary nodes, the field prediction results very accurate. However, since a large number of measurement points could be necessary, the measurement could be impracticable with an experimental apparatus.
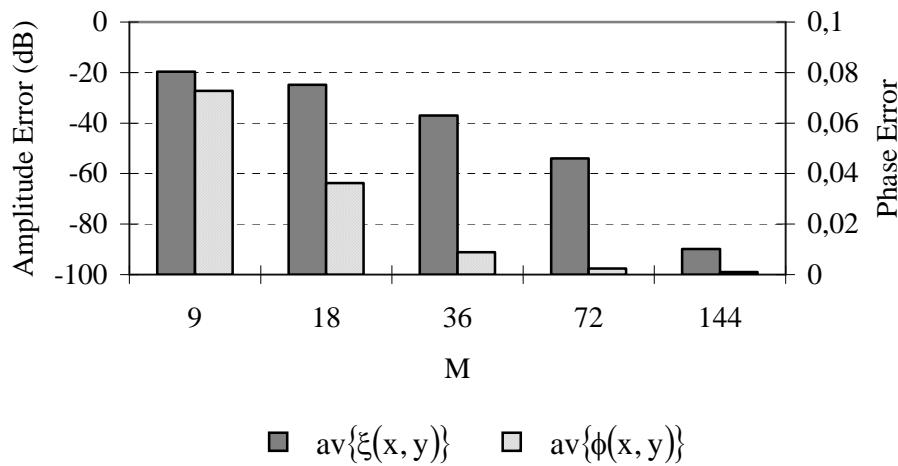
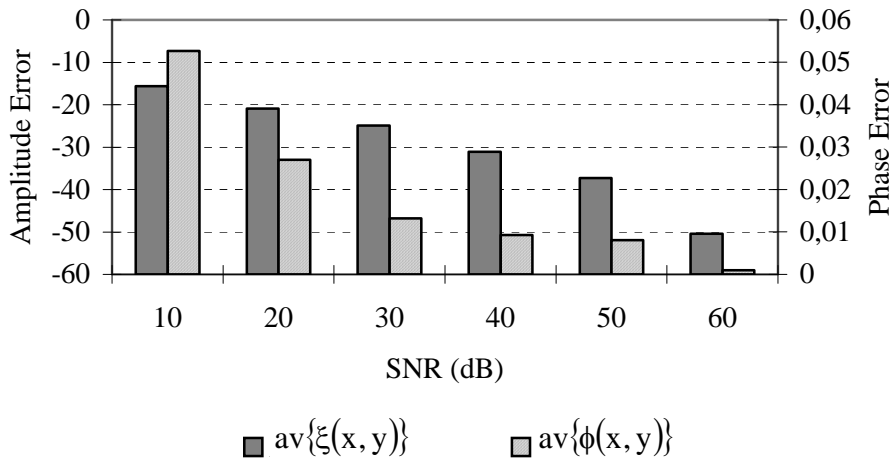**Fig. 5**. Prediction quality versus M. Average errors.

In order to verify if the number of measurement point can be reduced, the dependence of the field prediction on the number of measurement points is evaluated. To this aim, M equally spaced boundary nodes are taken into account as measurement points. Their positioning, along the squared surface, has been realized locating the first measurement point at the low left-corner of the measurement surface and then proceeding with a uniform spacing, in a clockwise direction. The values of the tangential component of the electric field on remaining boundary nodes are obtained by means of a quadratic interpolation of measured data.

M	$\xi(x_p, y_p)$
144	-120 dB
72	-50.2 dB
36	-30.2 dB
18	-25.8 dB
9	-21.8dB

Tab. I Estimation of the peak amplitude (inside the biological body) versus M. Amplitude error.

Figure 5 gives the average values of the error figures for different values of M. In particular, starting from one half until one sixteenth ($M = 9$) of boundary nodes have been considered. Whatever the

value of M is, the amplitude of the electric field is well estimated with an average error $av\{\xi(x,y)\} \leq$ -19.6dB and the phase is predicted with an average error $av\{\phi(x,y)\} \leq 0.072$.

Fig. 6 Prediction quality versus signal-to-noise ratio (SNR). Average errors.

Moreover, the value of the amplitude peak (i.e, the maximum amplitude of the electric field inside the biological structure) is satisfactorily estimated (see Table I) and always the peak position, (x_p, y_p), is correctly located.

In the third numerical example, the robustness of the proposed technique to noisy measurement data is investigated. In order to simulate the presence of a white gaussian noise, a complex quantity $\zeta^{noise}(\mathbf{r})$, whose real and imaginary parts are gaussian variables characterized by zero mean value and variance depending on the fixed signal-to-noise ratio (SNR), is added to the measurement data. For this case, input data are synthetically computed by means of the method of moments [7].
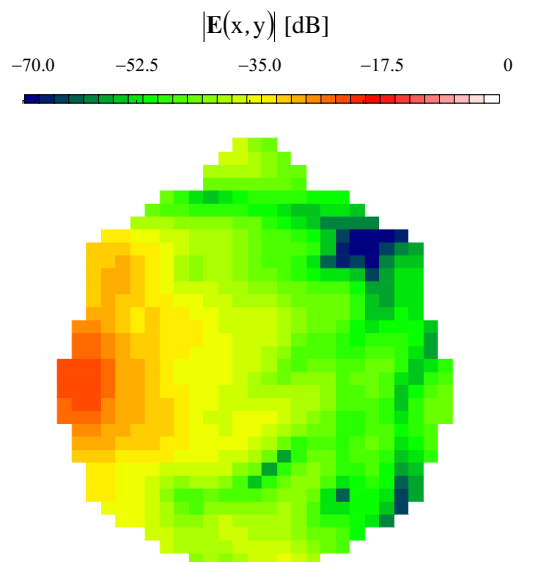
Fig. 7 Distribution of the field amplitude (SNR = 10dB).

Figure 6 shows average amplitude and phase errors for different values of the SNR. When SNR $\geq$ 20dB the average amplitude error results lower than –20.9dB. For the range of values, the phase error is lower than 0.027. On the other hand, when the signal-to-noise ratio further reduces, the

performances of the proposed approach decrease. The electric field is no longer well estimated, in particular at those regions where the amplitudes of the induced field are negligible with respect to the amplitude peak ($\xi(x_n, y_n) < \frac{1}{100} \xi(x_p, y_p)$).

Nevertheless, the location of the amplitude peak is correctly detected and its value estimated with an error lower than –18.7dB when SNR = 10dB (Figure 7).

Finally, the influence of an incorrect positioning of the measurement system is assessed. Numerically, this situation results in a measurement contour different from the one used to generate the input data. By a numerical point of view, this condition is simulated by considering, besides to the original measurement points $\{(x_m, y_m), m=1,...,M\}$, M of *false* observation points $(\tilde{x}_m, \tilde{y}_m)$ whose position is randomly chosen so that the following condition is fulfilled

$$(\tilde{x}_m, \tilde{y}_m) \in C_R(x_m, y_m) \qquad m = 1,..., M \qquad (11)$$

where $C_R(x_m, y_m)$ is a circle $R = t \cdot \nu^{max}$ ($t \in [0 \div 1]$) in radius, centered at the m-*th* measurement point; $\nu^{max} = \Delta_b / 2$ approximates the maximum error of the measurement system and is related to the accuracy of experimental positioning apparatus (which strongly depends on the application, but generally it is lower than few millimeters [31]). Then, measured data collected at $(\tilde{x}_m, \tilde{y}_m)$ $m = 1,..., M$ are assumed as input data at (x_m, y_m) $m = 1,..., M$. Table II gives error statistics for different value of the positioning parameter, t.

t	$av\{\xi(x, y)\}$	$av\{\phi(x, y)\}$	$\xi(x_p, y_p)$
0.1	-61.0 dB	$2.77 \cdot 10^{-4}$	-55.4 dB
0.2	-54.8 dB	$5.98 \cdot 10^{-4}$	-53.2 dB
0.3	-51.6 dB	$7.62 \cdot 10^{-4}$	-51.0 dB
0.4	-51.3 dB	$1.05 \cdot 10^{-3}$	-43.7 dB
0.5	-47.3 dB	$1.22 \cdot 10^{-3}$	-42.6 dB
0.6	-43.8 dB	$1.25 \cdot 10^{-3}$	-41.8 dB
0.7	-43.9 dB	$1.65 \cdot 10^{-3}$	-41.0 dB
0.8	-43.9 dB	$1.87 \cdot 10^{-3}$	-40.7 dB
0.9	-43.1 dB	$2.93 \cdot 10^{-3}$	-39.9 dB
1.0	-40.8 dB	$2.84 \cdot 10^{-3}$	-38.0 dB

Tab. II Average amplitude error, $av\{\xi(x, y)\}$, average phase error, $av\{\phi(x, y)\}$, and error in the prediction of the amplitude peak, $\xi(x_p, y_p)$, for various incorrect positioning.

For completeness Figures 8(*a*), 8(*b*) and 8(*c*) give the distributions of $\xi(x,y)$ when $t = 0.1$, $t = 0.5$ and $t = 1.0$, respectively. For all configurations, the electric field is accurately estimated inside the whole biological structure. The average amplitude error is always lower than -40.8dB and

$\text{av}\{\phi(x,y)\} < 2.84 \cdot 10^{-3}$. Moreover, the amplitude peak is correctly detected and its value well predicted ($\xi(x_p, y_p) \le -38\text{dB}$) for each value of t.

(a)

(b)

(c)
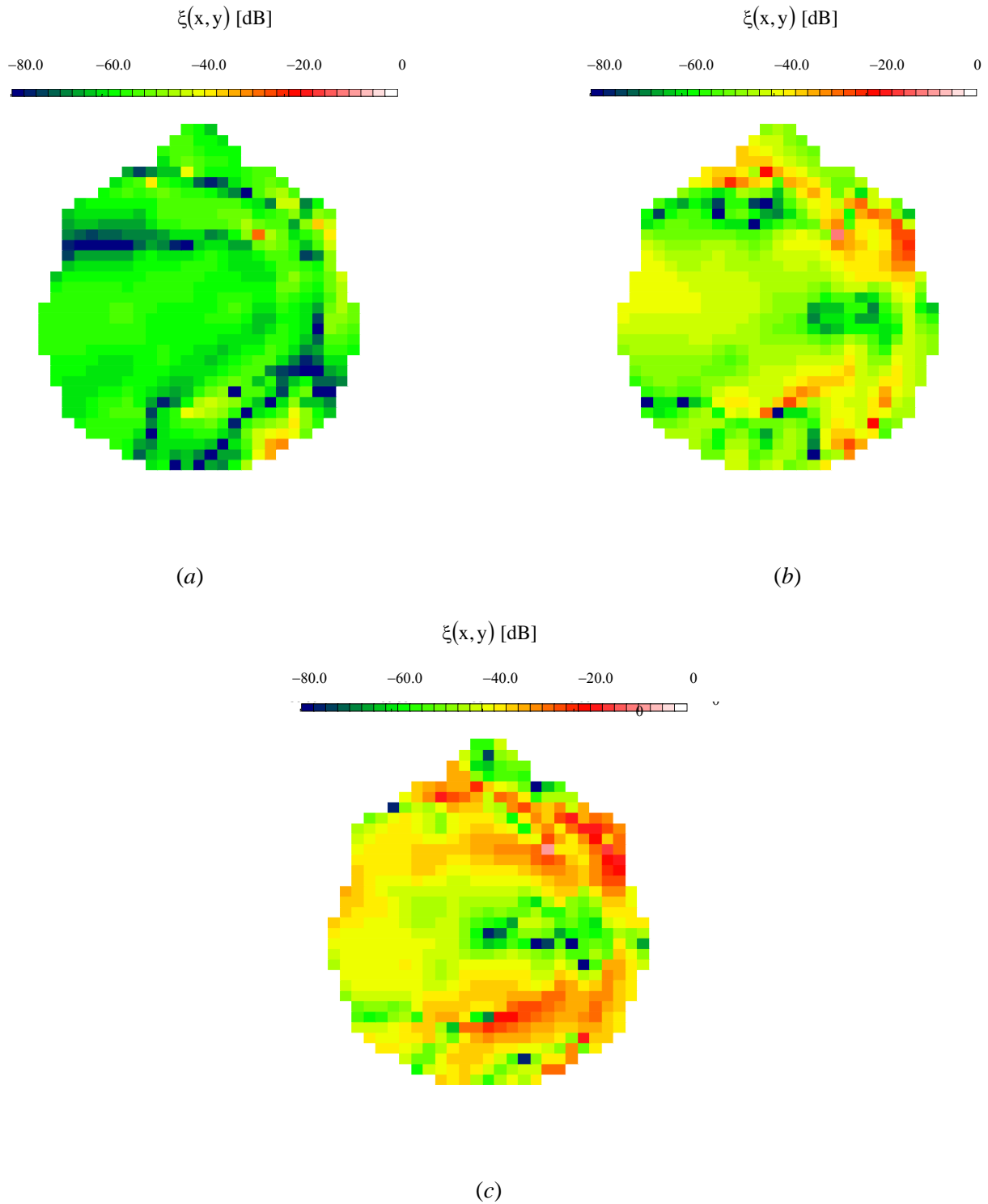
Fig. 8 Error in the estimation of the electric field amplitude: (*a*) t = 0.1, (*b*) t = 0.5 and (*c*) t = 1.0.

IV. CONCLUSIONS

In this paper, a finite element procedure, based on a boundary value approach, for the evaluation of the electromagnetic exposure in biological phantoms has been presented. Starting from the knowledge of the tangential component of the electric field at a number of points around the

10

biological structure, the electric field distribution has been estimated by solving a suitably defined boundary value problem. It allows to avoid the characterization of the electromagnetic source and to evaluate the electromagnetic exposure when the illuminating source is completely unknown or when its numerical model is not available.

The effectiveness of the proposed technique has been firstly checked, by considering numerical examples for which analytical reference solutions were available, and further assessed by analyzing a more complicate two dimensional geometry. It results a very high accuracy when measurement points are coincident with all boundary nodes. The use of a lower number of measurement points and the accuracy achievable in this case have been also evaluated. Moreover, the effects of noisy measurement data has been taken into account and good results have been obtained for signal-to-noise ratios greater or equal to 20dB. Finally, the effectiveness of the boundary value approach to errors in the positioning of the measurement system has been assessed.

REFERENCES

[1]. H. R. Chuang and K. M. Chen, "A numerical method for the computation of induced currents inside 3-D heterogeneous biological bodies by ELF-LF electric fields," *IEEE Trans. Biomedical Eng.*, vol. 36, pp. 628-634, 1989.

[2]. R. G. Olsen, S. L. Backus and R. D. Steam, "Development and validation of software for predicting ELF magnetic fields near power lines," *IEEE Trans. on Power Deliv.*, vol. 10, pp. 1525-1534, 1995.

[3]. T. W. Dawson and M. A. Stuchly, "High resolution organ dosimetry for human exposure to low frequency magnetic fields," *IEEE Trans. Magnetics*, vol. 34, pp. 1-11, 1998.

[4]. N. C. Skaropoulos, M. P. Ioannidou and D. P. Chrissoulidis, "Induced EM field in a layered eccentric spheres model of the head: plane-wave and localized source exposure," *IEEE Trans. Microwave Theory Tech.*, vol. 44, pp. 1963-1973, 1996.

[5]. R. W. P. King, "Electric fields induced in cells in the bodies of amateur radio operators by their transmitting antennas," *IEEE Trans. Microwave Theory Tech.*, vol. 48, pp. 2155-2158, 2000.

[6]. X. K. Kang, L. W. Li, M. S. Leong and P. S. Kooi, "Specific absorption rate distributions in a multilayered spheroidal human head model exposed to mobile dipoles," *Radio Science*, vol. 35, pp. 247-256, 2000.

[7]. K. L. Virga, Y. Rahmat-Samii, "Efficient wide-band evaluation of mobile communications antennas using Z or Y matrix interpolation with the method of moment," *IEEE Trans. Antennas Propagat.*, vol. 47, pp. 65-76, 1999.

[8]. K. D. Paulsen, P. M. Meaney, M. J. Moskowitz and J. M. Sullivan, "A dual mesh scheme for finite element based reconstruction algorithms," *IEEE Trans. Medical Imag.*, vol. 14, pp. 504-514, 1995.

[9]. P. M. Meaney, K. D. Paulsen, J. T. Chang, "Near-field microwave imaging of biologically-based materials using a monopole tranceiver system," *IEEE Trans. Microwave Theory Tech.*, vol. 46, pp. 31-45, 1998.

[10]. M. A. Mangoud, R. A. Abd-Alhameed and P. S. Excell, "Simulation of human interaction with mobile telephones using hybrid techniques over coupled domains," *IEEE Trans. Microwave Theory Tech.*, vol. 48, pp. 2014-2021, 2000.

[11]. X. Yuan, D. R. Lynch and J. W. Strohbehn, "Coupling of Finite Element and Moment Methods for Electromagnetic Scattering from Inhomogeneous Objects," *IEEE Trans. Antennas Propagat.*, vol. 38, pp. 386-393, 1990

[12]. H. Rogier, D. De Zutter and F. Olyslager, "Modelling Complex Structures by Combining the FE, FDTD and BIE Techniques," *IEEE AP-S Int. Symp.*, vol. 2, pp. 1062-1065, 1999.

[13]. M. A. Jensen and Y. Rahmat-Samii, "EM interaction of handset antennas and a human in personal communications," *Proc. of the IEEE*, vol. 83, pp. 7-17, 1995

[14]. L. Martens, J. DeMoerloose and D. De Zutter, "Calculation of the electromagnetic fields induced in the head of an operator of a cordless telephone," *Radio Science*, vol. 30, pp. 283-290, 1995.

[15]. M. Okoniewski and M. A. Stuchly, "A study of the handset antenna and human body interaction," *IEEE Trans. Microwave Theory Tech.*, vol. 44, pp. 1855-1864, 1996.

[16]. O. P. Gandhi, G. Lazzi and C. M. Furse, "Electromagnetic absorption in the human head and neck for mobile telephones at 835 and 1900 MHz," *IEEE Trans. Microwave Theory Tech.*, vol. 44, pp. 1884- 1897, 1996.

[17]. P. J. Dimbylow, "FDTD calculation of the whole-body average SAR in an anatomically realistic voxel model of the human body from 1MHz to 1GHz," *Phys. Med. Biol.*, vol. 42, pp. 479-490, 1997.

[18]. M. Okoniewski and M. A. Stuchly, "Modeling of interaction of electromagnetic field from a cellular telephone with hearing aids," *IEEE Trans. Microwave Theory Tech.*, vol. 46, pp. 1686-1693, 1998.

[19]. J, T. Rowley and R. B. Waterhouse, "Performance of shorted microstrip patch antennas for mobile communications handsets at 1800 MHz," *IEEE Trans. Antennas Propagat.*, vol. 47, pp. 815-822, 1999.

[20]. M. F. Iskander, Z. Yun and R. Quintero-Illera, "Polarization and human body effects on the microwave absorption in a human head exposed to radiation from handheld devices," *IEEE Trans. Microwave Theory Tech.*, vol. 48, pp. 1979-1987, 2000.

[21]. K. Caputa, M. A. Stuchly, M. Skopec, H. I. Bassen, P. Ruggera and M. Kanda, "Evaluation of electromagnetic interference from a cellular telephone with a hearing aid," *IEEE Trans. Microwave Theory Tech.*, vol. 48, pp. 2148-2154, 2000.

[22]. *Review of Radio Science 1996-1999*. Edited by W. R. Stone. Oxford Science Publication.

[23]. S. Caorsi and A. Massa, "A microwave-imaging technique for electromagnetic exposure prediction: preliminary results," *Microwave Opt. Tech. Lett.*, vol. 19, pp. 328-332, 1998.

[24]. S. Caorsi and A. Massa, "Electromagnetic field prediction inside biological bodies by using an inverse scattering procedure based on a statistical cooling algorithm," *Bioelectromagnetics*, vol. 21, p. 422-431, 2000.

[25]. S. Caorsi, E. Bermani and A. Massa, "A microwave imaging approach based on amplitude-only data for the reconstruction of the electromagnetic field induced in biological phantoms," *ACES Journal*, Special Issue on Bioelectromagnetics, vol. 16, pp. 79-89, 2001.

[26]. C. A. Balanis, *Advanced Engineering Electromagnetics*. John Wiley & Sons, New York, 1989.

[27]. J. Jin, *The Finite Element Method in Electromagnetics*. John Wiley & Sons, New York, 1993.

[28]. M. R. Hestenes and E. Stiefel, "Method of conjugate gradients for solving linear systems," *J. Res. Nat. Bur. Standards*, vol. 49, pp. 409-436, 1952.

[29]. H. Whitney, *Geometric Integration Theory*. Princeton, NJ: princeton University Press, 1957.

[30]. Z. S. Sacks, D. M. Kingsland, R. Lee, and J.-F. Lee, "A Perfectly Matched Anisotropic Absorber for Use as an Absorbing Boundary Condition", *IEEE Trans. Antennas Propagat.*, vol. 43, pp. 1460-1463, 1995.

[31]. A. Franchois, A. Joisel, Ch. Pichot, and J. Ch. Bolomey, "Quantitative microwave imaging with a 2.45-GHz planar microwave camera," *IEEE Trans. Medical Imag.*, vol. 17, pp. 550-561, 1998.